

## THE FOURTH VLBA CALIBRATOR SURVEY: VCS4

L. PETROV

NVI, Inc., 7257 Hanover Parkway, Suite D, Greenbelt, MD 20770; leonid.petrov@lpetrov.net

Y. Y. KOVALEV<sup>1</sup>

National Radio Astronomy Observatory, P.O. Box 2, Green Bank, WV 24944; and Astro Space Center of Lebedev Physical Institute, Profsoyuznaya 84/32, 117997 Moscow, Russia; ykovaev@nrao.edu

E. B. FOMALONT

National Radio Astronomy Observatory, 520 Edgemont Road, Charlottesville, VA 22903-2475; efomalon@nrao.edu

AND

D. GORDON

Raytheon/NASA Goddard Space Flight Center, Code 697, Greenbelt, MD 20771; dgg@leo.gsfc.nasa.gov

Received 2005 August 23; accepted 2005 October 22

### ABSTRACT

This paper presents the fourth extension to the VLBA Calibrator Survey, containing 258 new sources not previously observed with very long baseline interferometry (VLBI). This survey, based on three 24 hr Very Long Baseline Array observing sessions, fills remaining areas on the sky above declination  $-40^\circ$  where the calibrator density is less than one source within a  $4^\circ$  radius disk in any given direction. The share of these areas was reduced from 4.6% to 1.9%. Source positions were derived from astrometric analysis of group delays determined at 2.3 and 8.6 GHz frequency bands using the Calc/Solve software package. The VCS4 catalog of source positions, plots of correlated flux density versus projected baseline length, contour plots, and fits files of naturally weighted CLEAN images, as well as calibrated visibility function files, are available online and can be found using the search keyword “VCS4.”

*Key words:* astrometry — catalogs — surveys

*Online material:* color figure, machine-readable table

### 1. INTRODUCTION

This work is a continuation of the project of surveying the sky for bright compact radio sources. These sources can be used as phase-referencing calibrators for imaging of weak objects with very long baseline interferometry (VLBI) and as targets for space navigation, monitoring the Earth’s rotation, differential astrometry, and space geodesy. The method of VLBI, first proposed by Matveenko et al. (1965), allows us to determine the positions of sources with nanoradian precision ( $1 \text{ nrad} \approx 0.2 \text{ mas}$ ). Several catalogs were compiled combining observations under various programs. The catalog of sources observed under geodetic programs from 1979 through 2004, ICRF-Ext2 (Fey et al. 2004), contains the positions of 776 sources. In addition to that, the positions of 2247 sources were determined in the framework of the VLBA Calibrator Survey project: VCS1 (Beasley et al. 2002), VCS2 (Fomalont et al. 2003), and VCS3 (Petrov et al. 2005). Since 364 sources are listed in both the ICRF-Ext2 and the VCS catalogs, the total number of sources for which positions were determined with VLBI is 2659. Among them, 2269 sources, or 85%, are considered as acceptable calibrators: each has at least eight successful observations at both the X and S bands, and the semimajor axis of the error ellipse of their coordinates is less than  $25 \text{ nrad}$  ( $5 \text{ mas}$ ).

However, the sky coverage of these sources is not uniform. Successful phase referencing requires a calibrator within at least  $4^\circ$  from a target source with a precise position and known source structure. The probability of finding a calibrator from the combined ICRF-Ext2, VCS1, VCS2, and VCS3 catalogs within  $4^\circ$  of any target above  $-40^\circ$  declination is 95.4%. In this paper we

present an extension of the VCS catalogs, called the VCS4 catalog, mainly concentrating on the other 4.6% of the sky, where the source density is the lowest, and on the brightest sources with flat spectra previously not observed with VLBI under geodesy and astrometry programs. Since the observations, calibrations, astrometric solutions, and imaging are similar to those of VCS1–VCS3, most of the details are described by Beasley et al. (2002) and Petrov et al. (2005). In § 2 we assess an a priori probability of source detection. In § 3 we describe the strategy for selecting 412 candidate sources observed in three 24 hr sessions with the Very Long Baseline Array (VLBA) based on analysis of probabilities of source detection, which is a further development of the statistical approach for source selection introduced by Petrov et al. (2005). In § 4 we briefly outline the observations and data processing. We present the catalog in § 5 and summarize our results in § 6.

### 2. ASSESSMENT OF AN A PRIORI PROBABILITY OF SOURCE DETECTION

Having unlimited resources, one could try to observe all sources stronger than some limiting flux density. However, only sources with bright compact components can be detected with VLBI and may be useful for phase-referencing or geodetic applications. Kellermann et al. (1968) first showed that the distribution of sources over spectral index  $\alpha$  ( $F \propto \nu^{+\alpha}$ ) has two peaks: one near  $\alpha = -1$  (steep spectrum) and another near  $\alpha = 0$  (flat spectrum). Later, it was confirmed that extended objects dominate in the steep-spectrum population (see the review by Kellermann & Owen 1988). In compact regions, which have the synchrotron mechanism of emission, the peak in the spectrum caused by synchrotron self-absorption has frequencies higher than 1 GHz

<sup>1</sup> Jansky Fellow, National Radio Astronomy Observatory.

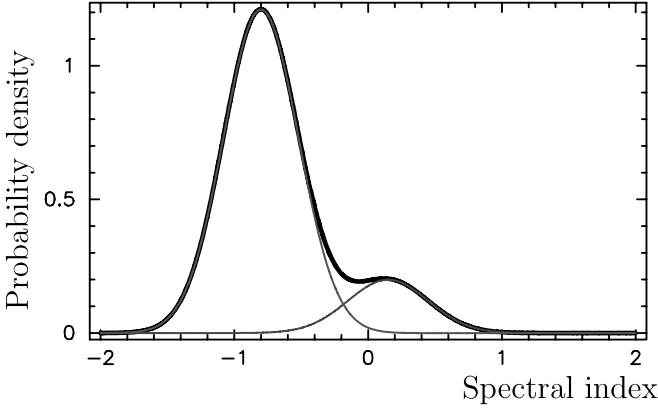


FIG. 1.—Probability density distribution at 8.6 GHz as a function of spectral index. The thin lines show the distribution of the steep-spectrum source population (*left curve*) and the flat-spectrum source population (*right curve*). [See the electronic edition of the *Journal* for a color version of this figure.]

due to the small size of the region (Slysh 1963). Thus, if the dominating emission comes from compact regions, the spectrum of the total flux density will be predominantly flat or inverted.

Let us determine the probability of detecting with the VLBA a source with a given total flux density and given spectral index. The empirical probability distribution function of sources in spectral indexes can be approximated as

$$P(\alpha) = (1 - a)N(\alpha, \alpha_s, \sigma_s) + aN(\alpha, \alpha_f, \sigma_f), \quad (1)$$

where  $a$  is the share of the flat-spectrum population in the total population and  $N(\alpha, \alpha_0, \sigma_0)$  is the normal distribution with a maximum at  $\alpha_0$  and a dispersion  $\sigma_0^2$ . The first term,  $N_s(\alpha) = N(\alpha, \alpha_s, \sigma_s)$ , represents the probability distribution for steep-spectrum sources, and the second one,  $N_f(\alpha) = N(\alpha, \alpha_f, \sigma_f)$ , is for flat-spectrum sources. Using the results of Mingaliev et al. (2001) for the RATAN-600 simultaneous broadband spectra survey at centimeter wavelengths of sources around the north celestial pole, as well as 2.7 and 5 GHz data from the Wright & Otrupcek (1990) PKSCat90 catalog with a limiting flux density at 2.7 GHz of 250 mJy, we have found the following estimates of the distribution parameters:  $a = 0.15$ ,  $\sigma_f = 0.30$ ,  $\alpha_f = 0.15$ ,  $\sigma_s = 0.28$ , and  $\alpha_s = -0.80$ . Figure 1 shows the distribution.

If a source has a spectral index in the range of  $[\alpha, \alpha + d\alpha]$ , the ratio of the probability that it belongs to the flat-spectrum population,  $P_f(\alpha)$ , to the probability that it belongs to the steep-spectrum population,  $P_s(\alpha)$ , is equal to the ratio of their probability densities:

$$\frac{P_f(\alpha)}{P_s(\alpha)} = \frac{aN_f(\alpha)}{(1 - a)N_s(\alpha)}. \quad (2)$$

Since we assume that a source belongs either to the flat-spectrum population or to the steep-spectrum population,  $P_f(\alpha) + P_s(\alpha) = 1$ . Then we immediately find

$$P_f(\alpha) = \frac{aN_f(\alpha)}{(1 - a)N_s(\alpha) + aN_f(\alpha)}, \quad (3)$$

$$P_s(\alpha) = \frac{(1 - a)N_s(\alpha)}{(1 - a)N_s(\alpha) + aN_f(\alpha)}. \quad (4)$$

The probability that a given source will have a ratio  $r$  of the correlated flux density  $F_{\text{corr}}$  to the total flux density  $F_{\text{tot}}$  is quite different for these two populations. The results of Kovalev et al. (2005) of the 2 cm VLBA survey (Kellermann et al. 1998) and

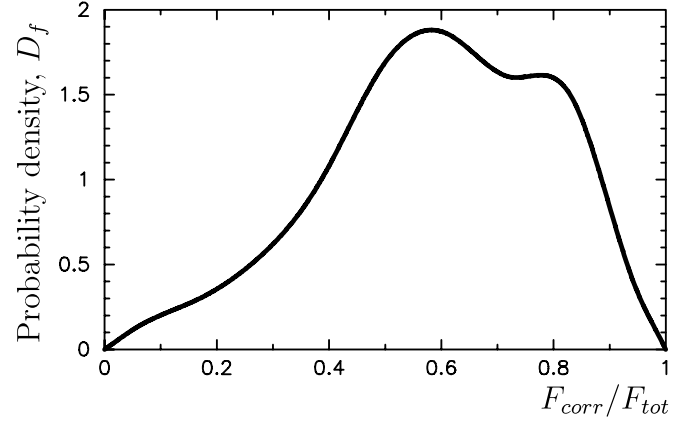


FIG. 2.—Probability density distribution at 8.6 GHz of the ratio of the correlated flux density at the baseline projections equal to the Earth radius to the total flux density among the flat-spectrum source population.

the results of the analysis of the VCS3 observing campaign provided us estimates of  $F_{\text{corr}}$  at baseline projections equal to the Earth radius. The total flux of these sources was measured with RATAN-600. The histogram of over 500 sources after smoothing and normalization gives us an estimate of the empirical probability density distribution of the ratio of correlated flux density at baseline projections equal to the Earth radius to the total flux density among the flat-spectrum source population (Fig. 2).

According to our previous experience in processing snapshot VLBA Calibrator Survey observations with an integration time of 4 minutes and a bit rate of 128 Msamples  $\text{s}^{-1}$  with good weather conditions, sources with correlated flux density greater than 60 mJy are reliably detected. We set the detection limit of the VLBA to  $F_{\text{lim}} = 70$  mJy in order to have a little allowance for possible pointing errors and higher than normal system temperature due to bad weather. The probability of having the correlated flux density greater than this limit,  $F_{\text{lim}}$ , i.e., the probability of detection for a source that belongs to the flat-spectrum population and has total flux density  $F_{\text{tot}}$ , is  $\rho_f(F_{\text{tot}}) = C_f(F_{\text{lim}}/F_{\text{tot}})$ , where  $C_f(r)$  is the cumulative probability function, defined as

$$C_f(r) = 1 - \int_0^r D_f(r) dr, \quad (5)$$

where  $D_f(r)$  is the probability distribution function of the ratio of the correlated flux density to the total flux density and  $r$  is the ratio of minimal detected correlated flux density to the total flux density. The plot of  $D_f(r)$  is shown in Figure 2, and the plot of  $C_f(r)$  is shown in Figure 3.

For steep-spectrum sources the probability density function of the ratio of the correlated flux density to the total flux density is not well known. According to our analysis of compact steep-spectrum sources detected in the VCS1–VCS3 experiments, we approximate

$$D_s(r) = \begin{cases} 20, & r < 0.05, \\ 0, & r \geq 0.05. \end{cases} \quad (6)$$

Analogously, we introduce the function  $C_s(r)$  for the steep-spectrum source population:

$$C_s(r) = 1 - \int_0^r D_s(r) dr. \quad (7)$$

Then, assuming the spectral index of a source is precisely known, the probability of being detected at 8.6 GHz for a source

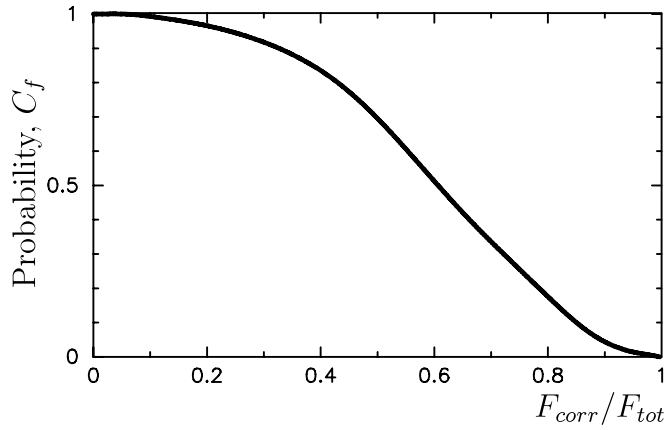


FIG. 3.—Cumulative probability function of the ratio of the correlated flux density to the total flux density among the flat-spectrum source population:  $C_f(r, F_{\text{corr}}/F_{\text{tot}}) = P_f(r \leq F_{\text{corr}}/F_{\text{tot}})$ .

with spectral index  $\alpha$  and total flux density  $F_0$  measured at frequency  $f_0$  is

$$P(F_0, f_0, \alpha) = P_f(\alpha)C_f\left(\frac{F_{\text{lim}}}{F_0 + (8.6/f_0)^\alpha}\right) + P_s(\alpha)C_s\left(\frac{F_{\text{lim}}}{F_0 + (8.6/f_0)^\alpha}\right). \quad (8)$$

Plots of the probability of being detected as a function of spectral index are presented in Figure 4. If no information about the spectral index is available, the estimate of the probability of detecting a source is

$$P(F_0) = \int_{-\infty}^{+\infty} \left[ P_f(\alpha)C_f\left(\frac{F_{\text{lim}}}{F_0 + (8.6/f_0)^\alpha}\right) + P_s(\alpha)C_s\left(\frac{F_{\text{lim}}}{F_0 + (8.6/f_0)^\alpha}\right) \right] d\alpha. \quad (9)$$

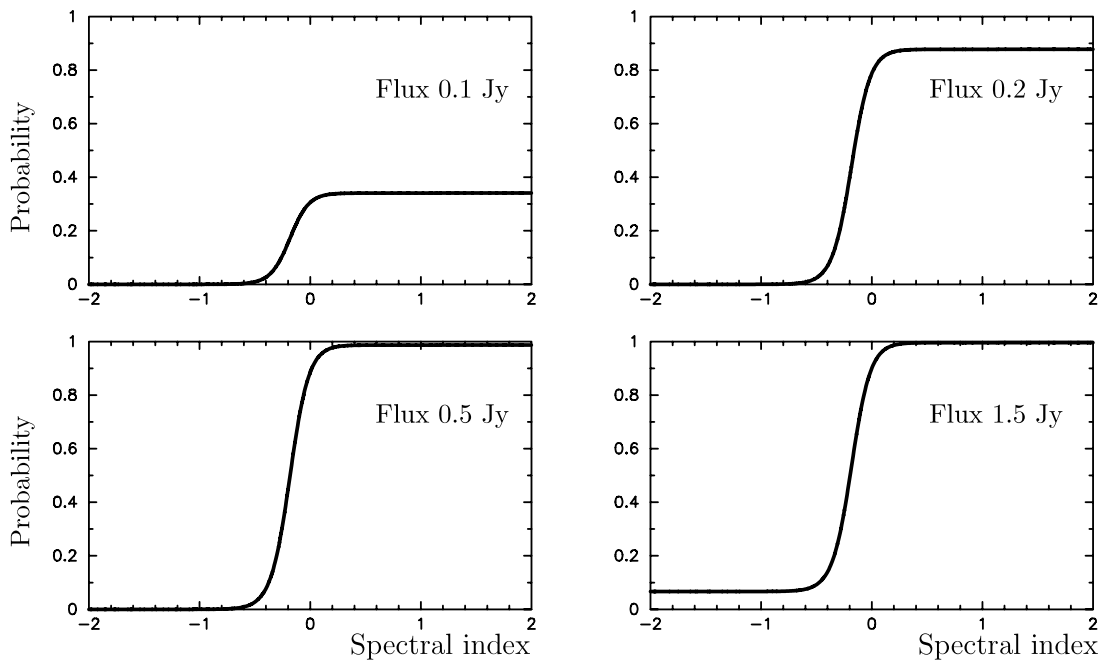


FIG. 4.—Probability of being detected at 8.6 GHz as a function of spectral index for sources with a 1.4 GHz flux density of 0.1, 0.2, 0.5, and 1.5 Jy.

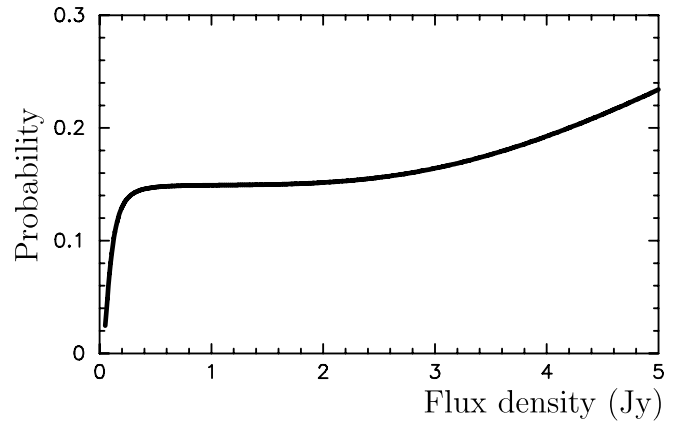


FIG. 5.—Probability of detection of a source with unknown spectral index as a function of total flux density at 1.4 GHz.

The plot of the probability of being detected for this case as a function of flux density is presented in Figure 5.

### 3. SELECTION OF CANDIDATE SOURCES FOR ZONES WITH LOW CALIBRATOR DENSITY

As the first step of source selection we computed the sky source density on a  $6' \times 6'$  grid and identified areas with declination more than  $-40^\circ$  and with no calibrator within a  $3^\circ$  disk. As the second step we selected all sources from the NRAO VLA Sky Survey catalog with flux density greater than 100 mJy at 1.4 GHz and Galactic latitude  $|b| > 1.5^\circ$  that either were not previously observed with VLBI under astrometry and geodesy programs or were observed but did not have enough data collected to be counted as calibrators. We used the CATS database (Verkhodanov et al. 1997) to gather all available flux density measurements and then computed a spectral index for each source. Sources with spectral index less than  $-0.5$  were deselected. We also deselected sources with extrapolated total flux density at 8.6 GHz less than 100 mJy. Sources for which the spectral index could not be reliably determined were removed from the list of

candidates if they had flux densities at 1.4 GHz less than 200 mJy. We also removed pairs of sources if the distance between components was less than  $0''.083$ , since this usually indicates a source with extended structure. Those sources, which according to the NASA/IPAC Extragalactic Database<sup>2</sup> (NED; Eichhorn et al. 2002) were listed as Galactic objects, H II regions, or planetary nebulae, were removed as well. Finally, we generated the input list of 2479 candidates. For 1216 objects we had estimates of their spectral indexes, and we computed the a priori probability of their detection using expression (8). For other sources we computed this probability using expression (9). It should be mentioned that many sources have a variable flux density and spectral index. These variations were not taken into account in the evaluation of the probability distribution and in equation (8). This makes the estimates of the probability of detection somewhat less reliable.

If all these sources could be observed, the mathematical expectation of the area without a calibrator within a disk of radius  $4^\circ$  would be 0.57%. For economical reasons we were forced to reduce the list of candidates. In order to find a subset of  $N$  sources in such a manner that the area with source calibrator density less than one source in a disk of radius  $4^\circ$  would be minimal, we adopted the following iterative procedure: Initially, we selected all sources. For each point on the grid with declination more than  $-40^\circ$  that *before* the VCS4 campaign had no calibrators closer than  $4^\circ$ , we computed the probability of that point having no calibrator closer than  $4^\circ$  *after* the VCS4 observations as

$$H_{ij} = \prod_{k=1}^n [1 - P_i(\alpha, F)] d(i, j, k), \quad (10)$$

where  $d(i, j, k)$  is 1 if the distance between the point on the grid  $(i, j)$  and the  $k$ th source is less than  $4^\circ$ , and 0 otherwise. The sum

$$R = \sum_{\text{grid}} H_{ij} \quad (11)$$

is the mathematical expectation of the total area that has no calibrator within  $4^\circ$ .

Then, at each step of iteration for each source we compute  $R_k = \sum_{\text{grid}} R d(i, j, k) / [1 - P_i(\alpha, F)]$ , i.e., the contribution of the  $k$ th source to  $R$ . The source with the minimal contribution is removed, the probability  $H_{ij}$  is updated, and the procedure is repeated until  $N$  sources remain in the list.

We generated the final list of candidates by concatenating two lists: (1) a list of 300 sources selected according to the iterative process described above and (2) a list of 100 sources north of declination  $-30^\circ$  with the highest probability of detection; these are the strongest flat-spectrum sources previously not observed in geodetic VLBI mode. We also added 12 sources that had been previously observed and detected under geodetic programs but never imaged with the VLBA. Of them, five sources fell in the areas with no calibrators, and therefore were considered as belonging to list 1; the other seven sources were added to list 2. The mathematical expectation of the area that would remain with no calibrator after observing the final list of 412 objects was 1.77%.

The rationale for including the list of the 100 brightest sources is that the area of the sky without a calibrator within a disk of

radius  $4^\circ$  is reduced too slowly if the number of candidates is increased by beyond several hundred. For most geodetic applications, having a bright calibrator a little bit farther from the target is more important than having the calibrator closer but much weaker. On the other hand, for accurate phase referencing a relatively close, weak calibrator is often preferable to a stronger calibrator that is much farther away. So, some compromise is needed in order to improve the calibrator list.

#### 4. OBSERVATIONS AND DATA PROCESSING

The VCS4 observations were carried out in three 24 hr observing sessions with the VLBA on 2005 May 12, June 12, and June 30. Each target source was observed in two scans. The scan duration was 120 s for sources from the list of 107 bright objects and 235 s for other target sources. The target sources were observed in a sequence designed to minimize loss of time from antenna slewing. In addition to these objects, 93 strong sources were taken from the Goddard Space Flight Center astrometric and geodetic catalog 2004f\_astro.<sup>3</sup> Observations of three to four strong sources from this list were made every 1–1.5 hr during observing sessions. These observations were scheduled in such a way that at each VLBA station at least one of these sources was observed at an elevation angle of less than  $20^\circ$ , and at least one at an elevation angle greater than  $50^\circ$ . The purpose of these observations was to provide calibration for mismodeled atmospheric path delays and to tie the VCS4 source positions to the ICRF catalog (Ma et al. 1998). The list of troposphere calibrators<sup>4</sup> was selected among the sources that, according to the 2 cm survey results (Kovalev et al. 2005), showed the greatest compactness index, i.e., the ratio of the flux density of an unresolved detail to the total flux density at VLBA baselines. In total, 505 sources were observed. The antennas were on-source 60% of the time.

Similar to the previous VLBA Calibrator Survey observing campaign (Petrov et al. 2005), we used the VLBA dual-frequency geodetic mode, observing simultaneously at 2.3 and 8.6 GHz. Each band was separated into four 8 MHz channels (intermediate frequencies) that spanned 140 MHz at 2.3 GHz and 490 MHz at 8.6 GHz, in order to provide precise measurements of group delays for astrometric processing. Since the a priori coordinates of candidates were expected to have errors of up to  $30''$ , the data were correlated with an accumulation period of 1 s in 64 frequency channels in order to provide extra-wide windows for fringe searching.

Processing of the VLBA correlator output was done in three steps. In the first step the data were calibrated and fringed using the Astronomical Image Processing System (AIPS; Greisen 1988). In the second step data were imported to the California Institute of Technology DIFMAP package (Shepherd 1997), and images were produced using the optimized automated procedure originally suggested by G. Taylor (Pearson et al. 1994). We were able to reach the VLBA image thermal noise level<sup>5</sup> for most of our CLEAN images (Wrobel & Ulvestad 2005). Errors of our estimates of correlated flux density of sources brighter than 100 mJy are determined mainly by the accuracy of amplitude calibration, which for the VLBA, according to Wrobel & Ulvestad (2004), is at the level of 5% at 1–10 GHz. This estimate was confirmed by comparison of the correlated flux density with the single-dish flux density that we measured with RATAN-600 in 2005

<sup>3</sup> See <http://vlbi.gsfc.nasa.gov/solutions/astro>.

<sup>4</sup> See [http://vlbi.gsfc.nasa.gov/vcs/tropo\\_cal.html](http://vlbi.gsfc.nasa.gov/vcs/tropo_cal.html).

<sup>5</sup> See <http://www.vlba.nrao.edu/astro/obstatus/current/obssum.html>.

<sup>2</sup> See <http://nedwww.ipac.caltech.edu>.

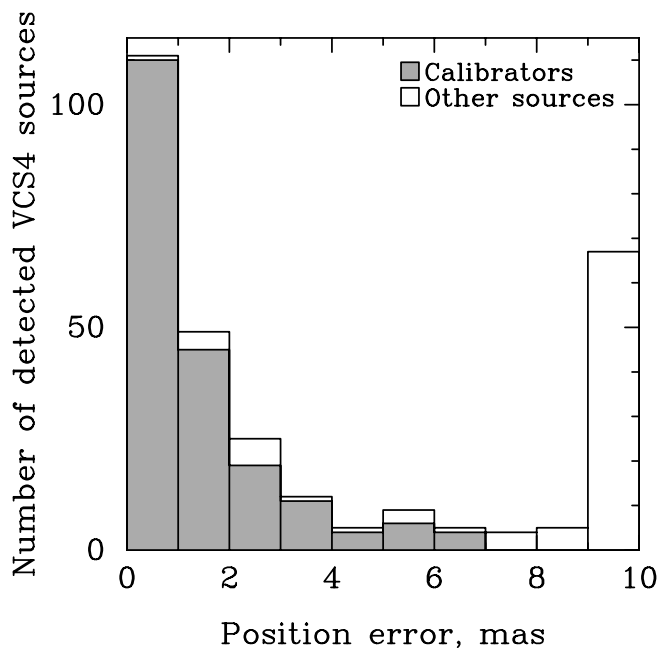


FIG. 6.—Histogram of the semimajor error ellipse of position errors. The last bin shows errors exceeding 9 mas.

March for slowly varying sources without extended structure. The methods of single-dish observations and data processing can be found in Kovalev et al. (1999). In the third step the data were imported to the Calc/Solve software, group-delay ambiguities were resolved, outliers were eliminated, and coordinates of new sources were adjusted using ionosphere-free combinations of X-band and S-band group-delay observables of the three VCS4 sessions, 15 VCS1–VCS3 experiments, and 3976 24 hr International VLBI Service for Astrometry and Geodesy (IVS) experiments<sup>6</sup> in a single least-squares solution. The boundary conditions that require zero net rotation of new coordinates of the 212 sources listed as defined in the ICRF catalog with respect to their positions from that catalog were imposed in order to select a unique solution of differential equations of photon propagation.

In a separate solution, coordinates of the 93 well-known tropospheric calibrators were estimated from the VCS4 observing sessions only. Comparison of estimates of coordinates of these sources with coordinates derived from analysis of the 3976 24 hr IVS experiments provided us a measure of the accuracy of the coordinates from the VCS4 observing campaign. The differences in coordinate estimates were used for computation of parameters  $a$  and  $b(\delta)$  of an error inflation model in the form  $[(a\sigma)^2 + b(\delta)^2]^{1/2}$ , where  $\sigma$  is an uncertainty derived from

<sup>6</sup> See <http://vlbi.gsfc.nasa.gov/solutions/2005c>.

the fringe amplitude signal-to-noise ratio using the error propagation law and  $\delta$  is the declination. More details about the analysis and imaging procedure can be found in Beasley et al. (2002) and Petrov et al. (2005). The histogram of source position errors is presented in Figure 6.

In total, 292 out of 412 sources were detected and yielded at least two good points for position determination. However, not all of these sources are suitable as phase-referencing calibrators or as targets for geodetic observations. Following Petrov et al. (2005), we consider a source suitable as a calibrator if (1) the number of good X-band/S-band pairs of observations is eight or greater in order to rule out the possibility of a group-delay ambiguity resolution error; and (2) the position error before reweighting is less than 5 mas following the strategy adopted in processing VCS observations. Only 196 sources satisfy these calibrator criteria. It should be mentioned that our criteria for suitability as a phase calibrator are rather conservative, and sources that fail these criteria may still be useful for some applications. Among 292 detected sources, 34 were previously observed but did not have enough observations before the VCS4 campaigns to be considered as calibrators. Of these 34 objects, new VCS4 observations of 27 of them provided enough information to classify them as calibrators.

Table 1 shows the statistics of the a priori and a posteriori detection rate. The a priori probability gives us a reasonable estimate of the detection rate. The sources from list 1 are weaker than the sources from list 2, and for 40% of them the integration time of 4 minutes was insufficient to qualify them as calibrators. The a posteriori detection rate turned out greater than the a priori rate, because we set the detection limit to 70 mJy when computing the a priori detection rate. In fact, we were able to detect sources with correlated flux densities as low as 50 mJy with an integration time of 4 minutes.

## 5. THE VCS4 CATALOG

The VCS4 catalog is listed in Table 2. Column (1) gives the source class “C” if the source can be used as a calibrator and a dash if it cannot. Columns (2) and (3) give the IVS source name (B1950.0 notation) and IAU name (J2000.0 notation). Columns (4) and (5) give the source coordinates at the J2000.0 epoch. Columns (6) and (7) give the inflated source position uncertainties in right ascension and declination (without the  $\cos \delta$  factor) in milliarcseconds, and column (8) gives the correlation coefficient between the errors in right ascension and declination. The number of group delays used for position determination is listed in column (9). Columns (10) and (12) give the estimate of the flux density in janskys integrated over the entire map at the X and S band, respectively. This estimate was computed as the sum of all CLEAN components if a CLEAN image was produced. If we did not have enough detections of visibility function to produce a reliable image, the integrated flux density was estimated as the median of the correlated flux density measured at projected spacings less than 25 and 7  $M\lambda$  for the X and S bands,

TABLE 1  
THE NUMBER OF OBSERVED AND DETECTED SOURCES

DATA	NO. SOURCES	NO. DETECTIONS	NO. CALIBRATORS	DETECTION RATE (%)		CALIBRATORS (%)
				A Priori	A Posteriori	
List 1 .....	305	199	117	45	65	38
List 2 .....	107	93	82	84	87	77
Total .....	412	292	199	57	71	48

TABLE 2  
THE VCS4 CATALOG

CLASS	SOURCE NAME		J2000.0 COORDINATES		ERRORS (mas)			No. OBS.	CORRELATED FLUX DENSITY (Jy)				BAND						
									8.6 GHz		2.3 GHz								
	(1)	(2)	(3)	R.A.	Decl.	(4)	(5)		(6)	(7)	(8)	(9)		Total	Unres.	Total	Unres.	(10)	(11)
—	0006–363	J0008–3601	00 08 33.661411	–36 01 25.05213	6.20	32.64	0.697	8	0.07	...	0.22	0.10	X/S						
C	0010+336	J0012+3353	00 12 47.382197	+33 53 38.47157	0.58	0.84	–0.508	41	0.16	0.13	0.07	0.06	X/S						
C	0012+319	J0015+3216	00 15 06.147414	+32 16 13.30953	0.33	0.55	–0.211	86	0.20	0.11	0.13	0.09	X/S						
C	0021–084	J0024–0811	00 24 00.672734	–08 11 10.04881	1.08	2.13	–0.252	31	0.10	0.08	0.09	0.07	X/S						
C	0024–114	J0026–1112	00 26 51.443027	–11 12 52.42503	0.96	1.68	0.219	30	0.11	0.05	0.19	0.09	X/S						
C	0032+612	J0035+6130	00 35 25.310617	+61 30 30.76144	0.93	0.60	0.200	71	0.14	0.06	0.23	0.07	X/S						
—	0033–088	J0035–0835	00 35 46.250383	–08 35 54.04258	0.83	1.57	–0.240	86	0.13	0.12	0.06	0.06	X						
C	0052–201	J0054–1953	00 54 32.948443	–19 53 01.00202	0.42	0.83	–0.091	59	0.16	0.10	0.20	0.05	X/S						
C	0052–125	J0055–1217	00 55 11.782596	–12 17 57.09709	0.25	0.46	–0.220	90	0.24	0.18	0.21	0.15	X/S						
—	0057+101	J0059+1022	00 59 46.769108	+10 22 40.42531	16.93	17.91	0.797	2	0.08	...	...	...	S						

NOTES.—Table 2 is published in its entirety in the electronic edition of the *Astronomical Journal*. A portion is shown here for guidance regarding its form and content. Units of right ascension are hours, minutes and seconds, units of declination are degrees, minutes and seconds.

respectively. The integrated flux density is the source total flux density with spatial frequencies less than  $4 M\lambda$  at the X band and less than  $1 M\lambda$  at the S band filtered out, or in other words, this is the flux density from all details of a source with size less than 50 mas at the X band and less than 200 mas at the S band. Columns (11) and (13) give the flux density of unresolved components estimated as the median of correlated flux density values measured at projected spacings greater than  $170 M\lambda$  for the X band and greater than  $45 M\lambda$  for the S band. For some sources no estimates of the integrated and/or unresolved flux density are presented, because either no data were collected at the baselines used in the calculations or these data were unreliable. Column (14) gives the data type used for the position estimation: X/S stands for an ionosphere-free linear combination of X and S wide-band group delays, X stands for X-band-only group delays, and S stands for S-band-only group delays. Some sources that yielded less than eight pairs of X- and S-band group-delay observables had two or more observations at the X and/or S band. For these sources either the X-band-only or S-band-only estimates of the coordinates are listed in the VCS4 catalog, whichever uncertainty is less.

In addition to this Table 2, the HTML version of this catalog is also posted on the Web.<sup>7</sup> For each source it has eight links: to a pair of postscript maps of the source at the X and S band; to a pair of plots of correlated flux density as a function of the length of the baseline projection to the source plane; to a pair of fits files with CLEAN components of naturally weighted source images; and to a pair of fits files with calibrated  $u-v$  data. The coordinates and the plots are also accessible from the NRAO VLBA Calibration Search Web site.<sup>8</sup>

Figure 7 presents examples of naturally weighted contour CLEAN images, as well as estimates of the correlated flux density versus projected spacings. The S-band data for the source J1531+3430 are an example of one of the weakest sources that we still were able to image. It turned out to be an object with an inverted radio spectrum of milliarsecond emission. The images of J0517–0520 show the compact structure with jet components that were detected on the level of several millijanskys per beam only. The source J0856–1105 has the highest VLBI flux den-

sity at the X band among all the new VCS4 objects and will be useful for geodetic applications along with a few tens of other compact VCS4 objects with high flux density at VLBA baselines.

## 6. SUMMARY

VCS4 has added 258 new sources not previously observed with VLBI. Among them, 199 sources turned out to be suitable as phase-referencing calibrators and as target sources for geodetic applications. The area with a source density of less than one calibrator within a disk of radius  $4^\circ$  in any given direction on the sky with  $\delta > -40^\circ$  was reduced from 4.6% to 1.9% (refer to Fig. 8 and Table 3). After processing the VCS4 experiments, the total number of calibrators has grown from 2268 to 2472. This pool of calibrators was formed from the analysis of 18 VLBI Calibrator Survey and 3976 24 hr IVS observing sessions.

The strategy of source selection based on a priori probabilities of source detection developed in this study was successful. The conservative a priori estimate of the detection rate was 57%, while the a posteriori detection rate is 70%. The a priori estimate of the area with a calibrator density of less than one object within a disk of radius  $4^\circ$  was 1.8%, while the a posteriori value is 1.9%.

The sky calibrator density for different radii of a search circle and for three different declination zones is presented in Table 3. A further search for new calibrators to decrease the area with insufficient sky calibrator density would be considerably less efficient, because the majority of the flat-spectrum sources in those areas have already been observed. The remaining sources are the steep-spectrum sources, sources with unknown spectral index, or very weak objects. According to Figure 5 the lack of information about spectral index of potential candidates makes the detection rate of almost any sample about the same.

At the same time, some relatively bright flat-spectrum sources remained in the zones where there is at least one calibrator in a disk of radius  $4^\circ$ . A sample of 675 such sources was observed in 2005 July with the VLBA in a follow-up VCS5 experiment (Y. Y. Kovalev et al. 2006, in preparation). The addition of these sources to the VLBA calibrator list will not affect the calibrator sky density with the search radius of  $4^\circ$  but will increase the density of calibrators with smaller search circles, which will be beneficial for many applications, for instance, the VLBI

<sup>7</sup> See <http://vlbi.gsfc.nasa.gov/vcs4>.

<sup>8</sup> See <http://www.vlba.nrao.edu/astro/calib>.

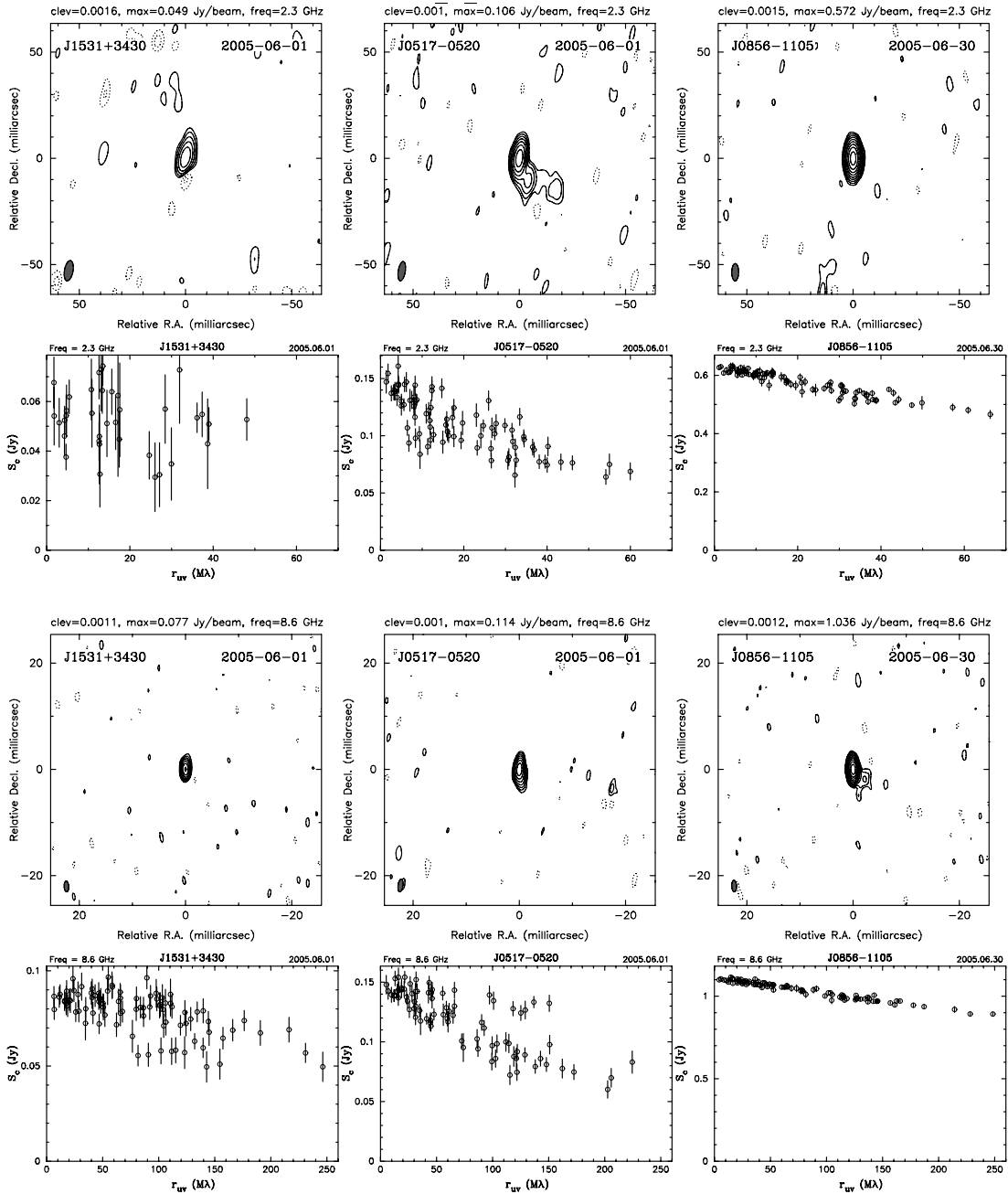


FIG. 7.—*First row*: Naturally weighted CLEAN images at the S band (2.3 GHz). The lowest contour levels (two steps) on the images are plotted at the “clev” levels ( $\text{Jy beam}^{-1}$ ), and the peak brightnesses at the “max” values ( $\text{Jy beam}^{-1}$ ). The dashed contours indicate negative flux. The beam is shown in the bottom left corner of the images. *Second row*: Dependence of the correlated flux density at the S band vs. projected spacings. The error bars were computed on the basis of the correlated flux density scatter around the mean value. *Third row*: Naturally weighted CLEAN images at the X band (8.6 GHz). *Fourth row*: Dependence of the correlated flux density at the X band on projected spacings.

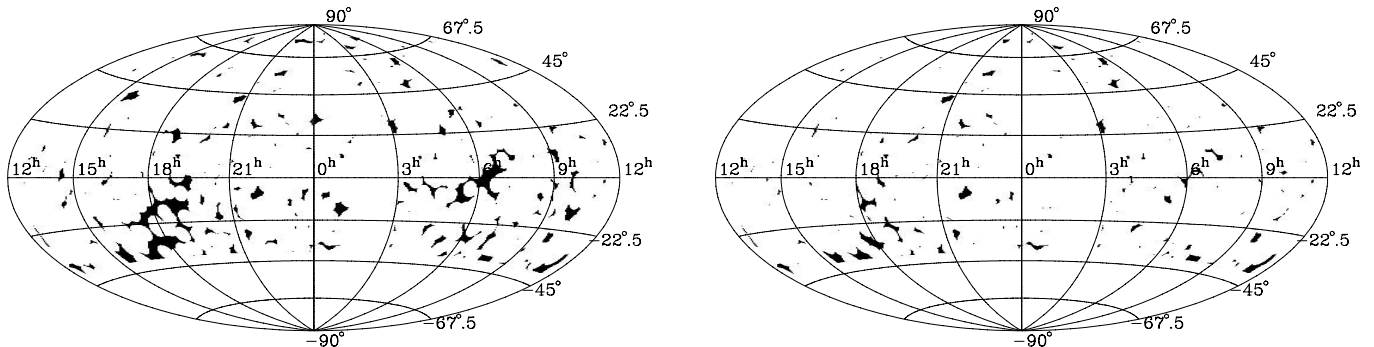


FIG. 8.—Source sky density before (*left*) and after (*right*) the VCS4 observing campaign. The areas above  $-40^\circ$  declination with a calibrator source density of less than one source within a  $4^\circ$  radius disk is shown in black.

TABLE 3  
 PROBABILITY OF FINDING A CALIBRATOR IN ANY GIVEN DIRECTION  
 WITHIN A CIRCLE OF A GIVEN RADIUS IN SELECTED  
 DECLINATION ZONES

SEARCH CIRCLE RADIUS (deg)	PROBABILITY (%)		
	$[-90^\circ, -40^\circ]$	$[-40^\circ, -30^\circ]$	$[-30^\circ, +90^\circ]$
4.0.....	63.6	92.2	98.6
3.5.....	55.4	86.0	96.0
3.0.....	44.1	76.4	89.7
2.5.....	33.2	56.6	77.9
2.0.....	22.7	46.6	60.7
1.5.....	13.6	29.4	40.0
1.0.....	6.3	14.2	20.1
0.5.....	1.6	3.7	5.4

NOTE.—All sources from the 3976 IVS astrometric and geodetic sessions and the 18 VCS1, VCS2, VCS3, and VCS4 experiments with the VLBA that are classified as calibrators are taken into account.

Exploration of Radio Astrometry (VERA) project (Honma et al. 2003).

New VCS4 detected sources were observed in 2005 with the Russian Academy of Sciences 600 m ring radio telescope RATAN for measurement of their *instantaneous* 1–22 GHz spectra (Y. Y.

Kovalev et al. 2006, in preparation). These data will allow us to determine the compactness of these sources and their accurate spectral indexes. Using this information one can further improve the estimate of the a priori probability of source detection with VLBI as a function of source flux and spectral index that will be essential for source selection in future surveys.

The National Radio Astronomy Observatory is a facility of the National Science Foundation, operated under cooperative agreement by Associated Universities, Inc. This work was done while L. P. and D. G. worked for NVI, Inc., and Raytheon, respectively, under NASA contract NAS5-01127. The authors are thankful to G. Lipunova for valuable comments. RATAN-600 observations were partly supported by the Russian State Program “Astronomy” and the Russian Ministry of Education and Science, the NASA JURRISS Program (project W-19611), and the Russian Foundation for Basic Research (projects 01-02-16812 and 05-02-17377). The authors made use of the database CATS (Verkhodanov et al. 1997) of the Special Astrophysical Observatory. This research has made use of the NASA/IPAC Extragalactic Database, which is operated by the Jet Propulsion Laboratory, California Institute of Technology, under contract with the National Aeronautics and Space Administration.

#### REFERENCES

- Beasley, A. J., Gordon, D., Peck, A. B., Petrov, L., MacMillan, D. S., Fomalont, E. B., & Ma, C. 2002, *ApJS*, 141, 13
- Eichhorn, G., Accomazzi, A., Grant, C. S., Kurtz, M. J., & Murray, S. S. 2002, *Ap&SS*, 282, 299
- Fey, A. L., et al. 2004, *AJ*, 127, 3587
- Fomalont, E., Petrov, L., MacMillan, D. S., Gordon, D., & Ma, C. 2003, *AJ*, 126, 2562
- Greisen, E. W. 1988, in *Acquisition, Processing, and Archiving of Astronomical Images*, ed. G. Longo & G. Sedmak (Naples: Oss. Astron. Capodimonte), 125
- Honma, M., et al. 2003, *PASJ*, 55, L57
- Kellermann, K. I., & Owen, F. N. 1988, in *Galactic and Extragalactic Radio Astronomy*, ed. G. L. Verschur & K. I. Kellermann (Dordrecht: Springer), 563
- Kellermann, K. I., Pauliny-Toth, I. I. K., & Davis, M. M. 1968, *Astrophys. Lett.*, 2, 105
- Kellermann, K. I., Vermeulen, R. C., Zensus, J. A., & Cohen, M. H. 1998, *AJ*, 115, 1295
- Kovalev, Y. Y., Nizhelsky, N. A., Kovalev, Yu. A., Berlin, A. B., Zhekanis, G. V., Mingaliev, M. G., & Bogdantsov, A. V. 1999, *A&AS*, 139, 545
- Kovalev, Y. Y., et al. 2005, *AJ*, 130, 2473
- Ma, C., et al. 1998, *AJ*, 116, 516
- Matveenko, L. I., Kardashev, N. S., & Sholomitskii, G. B. 1965, *Izv. VUZov. Radiofiz.*, 8, 651 (English transl. in *Soviet Radiophys.*, 8, 461 [1965])
- Mingaliev, M. G., Stolyarov, V. A., Davies, R. D., Melhuish, S. J., Bursov, N. A., & Zhekanis, G. V. 2001, *A&A*, 370, 78
- Pearson, T. J., Shepherd, M. C., Taylor, G. B., & Myers, S. T. 1994, *BAAS*, 185, 08.08
- Petrov, L., Kovalev, Y. Y., Fomalont, E., & Gordon, D. 2005, *AJ*, 129, 1163
- Shepherd, M. C. 1997, in *ASP Conf. Ser. 125, Astronomical Data Analysis Software and Systems VI*, ed. G. Hunt & H. E. Payne (San Francisco: ASP), 77
- Slysh, V. I. 1963, *Nature*, 199, 682
- Verkhodanov, O. V., Trushkin, S. A., Andernach, H., & Chernenkov, V. N. 1997, in *ASP Conf. Ser. 125, Astronomical Data Analysis Software and Systems VI*, ed. G. Hunt & H. E. Payne (San Francisco: ASP), 322
- Wright, A. E., & Otrupcek, R. 1990, *PKSCAT90 Radio Source Catalogue and Sky Atlas* (Epping: ATNF)
- Wrobel, J. M., & Ulvestad, J. S. 2005, *VLBA Status Summary* (Green Bank: NRAO)